Separation and Purification Technology 256 (2021) 117787

Contents lists available at ScienceDirect

Separation and Purification Technology

journal homepage: www.elsevier.com/locate/seppur

Highly crystalline ionic covalent organic framework membrane for nanofiltration and charge-controlled organic pollutants removal

Tongfan Chen [a,b], Bin Li [a,b,*], Wenbo Huang [a,b], Chunhui Lin [a,b], Guangshe Li [c], Hao Ren [c], Yue Wu [d], Shuhui Chen [d], Wenxiang Zhang [d,*], Heping Ma [d,*]

[a] State Key Laboratory of Luminescence and Applications, Changchun Institute of Optics, Fine Mechanics and Physics, Chinese Academy of Sciences, Changchun 130033, PR China
[b] University of Chinese Academy of Sciences, Beijing 100049, PR China
[c] State Key Laboratory of Inorganic Synthesis and Preparative Chemistry, College of Chemistry, Jilin University, Changchun 130012, PR China
[d] Shaanxi Key Laboratory of Energy Chemical Process Intensification, School of Chemical Engineering and Technology, Xi'an Jiaotong University, Xi'an 710049, PR China

ARTICLE INFO

Keywords:
Ionic 2D covalent organic framework
Microporous membrane
Organic pollutants
Nanofiltration
Selective molecular sieving

ABSTRACT

Organic pollutants are biological toxicity and should be removed from the environment. Membrane separation offers several advantages in organic pollutants removal such as high pollutants selectivity and high solvent permeability. Covalent organic framework membrane is regarded as an emerging porous membrane for nanofiltration owing to their permanent porosity and well-defined pore structure in various organic media. Herein, a self-standing 2D sulfonate anionic COF membrane with nanometer pore size and -SO_3Na groups has been successfully prepared. The surface charge combines with nanopore sieving property endow the COF membrane high nanofiltration separation performances and charge-controlled organic molecular separation. The anionic membrane can effectively intercept > 99% of cationic organic pollutants, while maintaining excellent solvent permeability due to its rigid porous structure and high porosity. The density functional theory (DFT) calculation provides further understanding on the charge-controlled separation in ionic nanoporous membranes. Our work may open up a new avenue for developing charged COF membrane for nanofiltration and organic pollutants separation applications.

1. Introduction

The occurrence of organic pollutants in the environment has raised global concern due to their potential ecological risks [1–3]. Organic pollutants tend to be resistant to biodegradation and many of them are biological toxicity. Sources of organic pollutants are synthetic chemical industry including dyes, pesticides, pharmaceuticals, detergent and organic solvents production [4–6]. Most wastewater post-treatment plants are not designed to completely eliminate organic compounds at low concentration, making the treatment process less effective to organic pollutants removal. Moreover, the above-mentioned chemical industrial wastewater usually contains high concentration of organic solvents, which makes the traditional nanofiltration (NF) membrane is less-effective for removing organic pollutants in complex wastewater systems. Thus, it is critical need to develop new-type membrane material for using in nanofiltration process containing organic solvents [7–9].

The applications of polymer membrane in organic solvents nanofiltration lags behind water purification and desalination mainly due to their poor stability (swelling or dissolution) in organic solvents. Moreover, the trade-off between membrane permeability and selectivity in traditional polymer membrane will be more serious under organic solvent filtration [10–14]. Recently, conjugated microporous polymer membranes have brought about widespread attention because of their extraordinary stability in organic solvent nanofiltration. The microporous polymer membranes used in NF process must possess excellent stability in a wide range of organic solvents with different polarities. All-rigid conjugated polymers with nanoporous structure exhibit apparent advantages for high flux NF and displaying remarkable solvent permeability [8,15,16]. However, if nanoporous polymer membranes want to achieve high-precision molecular sieving, the pore size of membranes must be precisely controlled. Till now, it is still a great challenge to obtain well-defined pore structure in amorphous polymer membrane

* Corresponding authors.
E-mail addresses: libinteacher@163.com (B. Li), zhangwenxiang@xjtu.edu.cn (W. Zhang), maheping@mail.xjtu.edu.cn (H. Ma).

https://doi.org/10.1016/j.seppur.2020.117787
Received 3 June 2020; Received in revised form 13 September 2020; Accepted 21 September 2020
Available online 28 September 2020

[17–19].

Covalent organic frameworks (COFs) emerged as new crystalline porous materials have attracted widespread attention because of their well-ordered nanopore and easy-to-functionalize pore environment [20–22]. Moreover, the pore structure of COFs is permanent stable in both polar and nonpolar organic solvents [23,24]. Therefore, COFs are considered as promising candidates for membrane materials used in both aqueous and organic solvents [25,26]. Recently, some COF membranes have been developed for high flux aqueous nanofiltration. The selective molecule separation in these COF films were achieved by size exclusion benefitting from their uniform pore sizes [27–29].

Integrating the ionic modules into membrane will endow fantastic functions for separation process such as charge-controlled molecular sieving [30–36]. Within charged microporous channel, the molecule transport in membrane will be dual-controlled by pore size and charge effect. Moreover, introducing charged site in membrane is more important for organic pollutants removal as most of organic pollutants such as dyes, pesticides and pharmaceuticals are ionic compounds [37–39]. Herein, we propose a 2D sulfonate anionic COF membrane with accessible ionic units and uniform nano channels for cationic organic pollutants removal (Fig. 1). The anionic COF membrane possesses permanent microporous structure in various solvents, and their charged nature can afford selective organic pollutants removal via charge-controlled separation.

2. Experimental section

2.1. Materials

General information: Unless otherwise noted, all chemical reagents and solvents from commercial sources were received and used without further purification. Twice-distilled water was used throughout all experiments. Solvents and reagents for synthesis were purchased from Sigma-Aldrich and Beijing chemical factory. Phloroglucinol, hexamethylenetetramine (HMTA, 99%), trifluoroacetic acid (99%), sodium 2,5-Diaminobenzenesulfonate (Pa-SO_3Na), p-toluenesulfonic acid (PTSA, 99.9%), Methylene blue (MB, 99%), Ethidium bromide (EB, 99%) (3,8-diamino-5-ethyl-6-phenyl -phenanthridinium bromide), Nile red (NR, 99%), p-Nitroaniline (NA, 99%), methyl orange (MO, 99%), fluorescein sodium salt (FSs, 99%), Sodium dodecyl sulfate (SDS, 99%), Sodium dodecyl benzene sulfonate (SDBS, 99%), Perfluorooctanesulfonic acid potassium salt (FC-80, 99%), Dodecyl trimethyl ammonium bromide (DTAB, 99%), Octadecyltrimethylammonium bromide (OTAB, 99%), Stearyldimethylbenzylammonium chloride (SDBAC, 99%), sodium chloride (NaCl, 99.9%). N,N-dimethyl formamide (DMF, 99.9%), hydrochloric acid (HCl, 6 M aqueous solution), dichloromethane (99%), acetone (99%), methanol (99%), ethanol (99%), n-propanol (98%), n-butanol (98%), 1-Pentanol (98%), n-Hexyl alcohol (99%), acetonitrile (99%), acetone (99%), tetrahydrofuran (98%), 1,4-dioxane (99%), N,N-dimethylacetamide (99%).

2.2. Preparation of TpPa-SO_3Na membrane

TpPa-SO_3Na membrane was prepared according to the previous literature reported methods with little modification [40]. In the typical route of interfacial synthesis, TpPa-SO_3Na membrane was prepared in a glass beaker. A schematic of the fabrication steps is shown in Fig. 1a, b, and the photographs of interfacial synthesis of TpPa-SO_3Na can see Fig. S3.

2.3. Characterization

Fourier transform infrared (FT-IR) spectra were performed using an IFS 66V/S Fourier trans-form infrared spectrometer. Powder X-ray diffraction (PXRD) measurement was carried out on a Riguku D/MAX2550 diffractometer with Cu-K a radiation operating at a voltage of 50 kV and a current of 200 mA. Scanning electronic microscopy (SEM) images were recorded by a Hitachi S-4800 microscope. Transmission electron microscopy (TEM) images were measured on a JEM-2010 field-emission transmission election microscope made by Japanese JEOL Company. The energy dispersive spectrometer (EDS) analysis was conducted by Aztec X-maxN (TESCAN Corporation, Czech Republic). The UV–vis absorption spectra of different dye solutions were performed with a Shimadzu UV-3101 PC double-beam ultraviolet–visible spectrophotometer. The Nitrogen adsorption/desorption isotherm analyse was measured on a Quantachrome Autosorb iQ2 analyzer. N_2 adsorption/desorption measurements were carried out at 77 K. Ultra-high-purity grade N_2 gas was used for adsorption measurements. Liquid nitrogen bath was utilized to control the temperature at 77 K. Initially, the sample was fully ground into powder. And prior to gas adsorption treatment

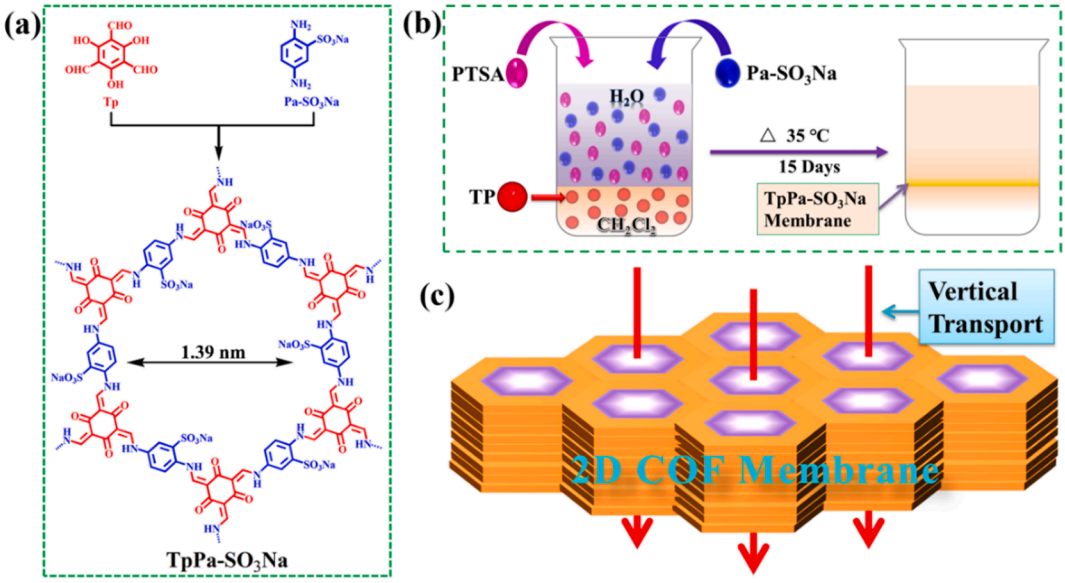

Fig. 1. (a) Schematic diagram of prepare TpPa-SO_3Na membrane by condensation reaction of sodium 2,5-diaminobenzenesulfonate (Pa-SO_3Na) and 1,3,5-triformylphloroglucinol (Tp); (b) Schematic diagram of interfacial growth method for fabricating TpPa-SO_3Na membrane. (c) The model of mass transport across 2D COF membrane along the vertically aligned nano channels.

sample was degassed at 160 °C for 12 h under vacuum. Surface area was calculated using Brunauer-Emmett-Teller (BET) model and corresponding pore size distribution was calculated using the non-localized density functional theory (NLDFT). Zeta-potential distribution was measured on a Malvern Zetasizer Nano ZES analyzer (U.K.). Contact angle tests were performed with a KRUSS DSA100 optical contact angle measuring device (Germany). The surface tension of surfactant solutions was measured using a KRUSS DSA100 device (Germany).

2.4. Selective organic micropollutants separation experiments

All the organic micropollutants separation experiments were performed at room temperature condition. Organic micropollutants are dissolved in water or methanol as stock solution. The concentration of organic micropollutants stock solutions was adjusted according to the different solutes. For example, the concentration of all dye stock solutions is fixed at 50 μM, while the concentration of surfactants stock solutions is determined according to their respective saturated micelle concentrations. The selective separation performance of TpPa-SO_3Na membrane towards organic micropollutants was evaluated by filtering a series of micropollutants stock solutions through the membrane at 0.5 bar pressure. Typically, the initial 5 mL organic micropollutants filtrate was collected for interception analysis. For organic dyes, the concentration of dye at initial condition and in the filtrate was monitored via a double-beam UV–vis spectrometer at a wavelength of maximum absorbance [663 nm for Methylene Blue (MB); 283 nm for Ethidium Bromide (EB); 263 and 552 nm for Nile Red (NR); 369 nm for p-Nitroaniline (NA); 462 nm for Methyl Orange (MO); 487 nm for Fluorescein Sodium salt (FSs)]. Unlike organic dyes, for surfactants, there is a functional relationship between the concentration of the solution and its surface tension. Therefore, we can calculate the concentration of the surfactant in the filtrate according to the surface tension value of the filtrate, and then the rejection efficiency of the membrane to the surfactants can be obtained.

The rejection efficiency of organic micropollutants was calculated as follows [40]:

$$\text{Rejection efficiency } (\%) = (C_0 - C_1)/C_0 \times 100 \quad (1)$$

where C_0 and C_1 were the concentration of organic micropollutants in stock solution and filtrate, respectively.

2.5. Solvent flux measurements

In order to evaluate the solvent flux of TpPa-SO_3Na membrane to pure solvents of different polarity and molecular weight. A series of TpPa-SO_3Na membranes with a diameter of 2.5 cm were placed on sand core filter unit (1.77 cm^2 active area) and all solvents permeation were performed under 0.5 bar upstream pressure. Solvent flux values reported were the average of triplicate experiments conducted with three different samples.

Solvent flux (J) was calculated by measuring permeate volume (V) per unit area (A) per unit time (t) according to the following equation:

$$J = V/A\hat{A}\cdot t \quad \text{in liters per square meter hour } (L\ m^{-2}\ h^{-1})$$

Permeance (P) was calculated according to the following equation:

$$P = V/A\hat{A}\cdot t\hat{A}\cdot \Delta p \text{ in liters per square meter hour bar } \left(L\ m^{-2}\ h^{-1}\ bar^{-1}\right)$$

The effect of membrane thickness and operation pressure to flux was also evaluated, respectively.

2.6. Cycle study of TpPa-SO_3Na membrane for dyes interception efficiency

A cycling experiment of TpPa-SO_3Na membrane for MB interception was carried out as follows. In the beginning, a anionic MB solution was filtered through TpPa-SO_3Na membrane and the filtrate was collected for rejection analysis. Then the membrane, after intercepting anionic MB, was rinsed thoroughly with aqueous NaCl solution (1.0 mol L^{-1}) at room temperature. Subsequently, the filtration experiment of TpPa-SO_3Na membrane for MB solution was repeated several times using the same membrane under the same conditions as above. Finally, these filtrates were monitored using a double-beam ultraviolet–visible spectrometer to evaluate the rejection efficiency of cycle experiment.

2.7. The time course of dyes rejection efficiency

The time course of rejection experiment of TpPa-SO_3Na membrane for dyes was carried out as follows. The time course of dyes rejection analysis was performed by filtering 50 μM dye solution through TpPa-SO_3Na membrane. Typically, 50 μM MB aqueous was charged to a sand core filter unit with TpPa-SO_3Na membrane and the filtrate was collected at intervals of 1 h. Then the absorbance of each filtrate at different points in time was measured. According to the Eq. (1) above, the rejection values were calculated. Finally, the time course of dyes rejection efficiency was obtain.

All dye solutions filtration were performed under 0.5 bar upstream pressure while maintaining 300 r.p.m as the stirring speed. Dyes rejection values reported were the average of triplicate experiments conducted with three different TpPa-SO_3Na membrane samples.

3. Results and discussion

3.1. General characterization of TpPa-SO_3Na membrane

In order to obtain large-scale crystalline anionic 2D COF membrane, we optimized two-phase interfacial crystallization approach reported by previous literature [40]. We modified the sulfonic acid group of the diaminobenzenesulfonic acid monomer into its sodium salt as diaminobenzenesulfonic acid showed low reactivity due to the strong intramolecular hydrogen bonding between sulfonic acid and amino group (Fig. S1). This modification not only breaks the hydrogen bond between amino group and sulfonic acid, but also greatly improves the solubility of aromatic amines in water (Fig. S2). In two-phase interfacial polymerization, the solubility of aromatic amines in water is very important because it determines the quality of the reaction interface. After screening monomer concentration, buffer layer thickness, catalyst amount and reaction times in interfacial polymerization, a large-scale crystalline anionic COF membrane with smooth surface on both sides are obtained (Fig. 2a, b and Fig. S3, S4). The cross-section SEM image displayed that the edge of the membrane has a uniform thickness about 2.8 μm (Fig. 2b inset). The resulting membrane can be transferred to different substrates as you want. Fig. 2a shows the digital image of a large-scale TpPa-SO_3Na membrane transferred on a printing paper.

The FT-IR spectra of obtained TpPa-SO_3Na membrane and initial monomers were implemented to confirm the success of interfacial polymerization. As shown in Fig. 2c, the COF membrane exhibits typical stretching bands at 1596 and 1231 cm^{-1} derive from C═C and C—N, indicating the complete enol-to-keto tautomerization. Moreover, the —CHO group stretching bands of Tp (O═C—H at 2890 cm^{-1}, C═O at 1642 cm^{-1}) and the —NH_2 groups stretching bands of Pa-SO_3Na are disappeared (N—H at 3196, 3303 cm^{-1}), which suggest the polymerization is completed. In addition, the FT-IR peaks at 1027 and 1089 cm^{-1} together with a shoulder at 1443 cm^{-1} arised from the O═S═O stretching bands, verified the existence of -SO_3^- group in COF membrane [41,42]. To further prove the presence of -SO_3Na functional group in the membrane, the energy dispersive spectrometer (EDS) analysis was performed. As shown in Fig. 2d, the presence of sulfur (S) and sodium (Na) elements in the membrane confirmed the -SO_3Na group is retained during the reaction. Moreover, the atomic percentage of sulfur and sodium elements is very close to 1:1 (Inset in Fig. 2d), which means Na ions in -SO_3Na group are not replaced by the H of p-toluenesulfonic acid.

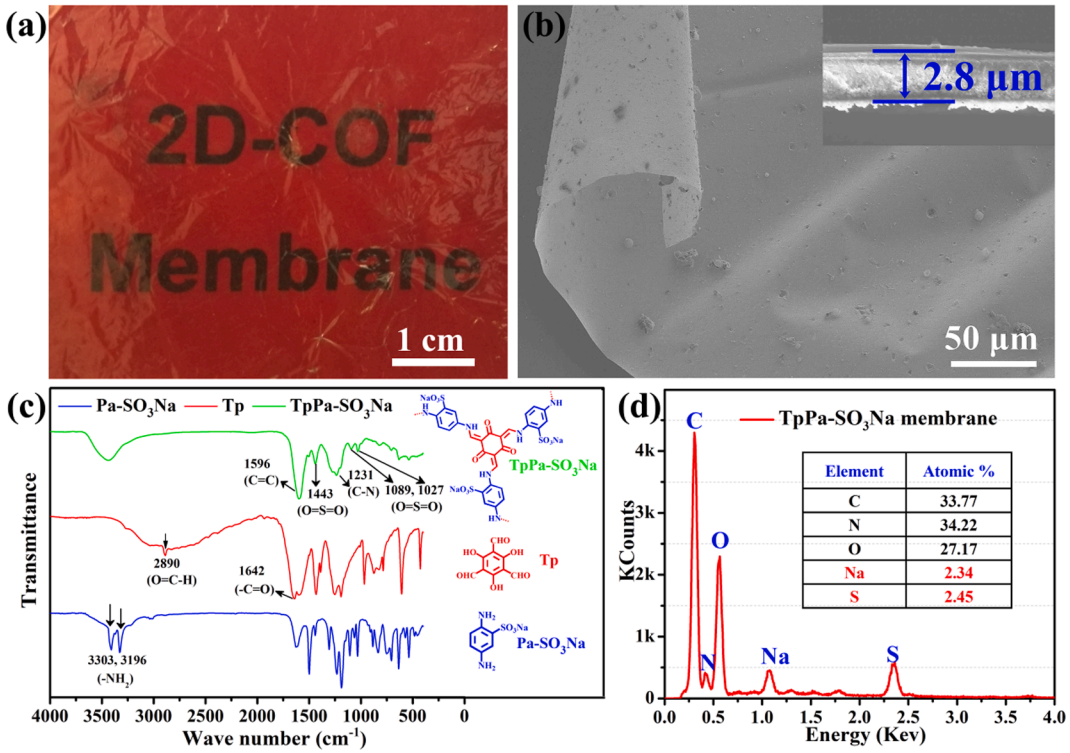

Fig. 2. (a) Optical image of TpPa-SO_3Na membrane; (b) Surface and Cross-sectional SEM image of TpPa-SO_3Na membrane; (c) FT-IR spectra of TpPa-SO_3Na, triformylphloroglucinol (Tp), and sodium 2,5-diaminobenzenesulfonate (Pa-SO_3Na); (d) EDS elemental analyses of TpPa-SO_3Na membrane (C, N, O, Na, and S).

To gain a deep insight into the pore structure of TpPa-SO_3Na membrane, the transmission electron microscopy (TEM) analysis was performed. As displayed in Fig. 3a, b, the clear lattice fringes in TEM images reveal the high crystallinity of TpPa-SO_3Na membrane. The diameter of the ordered pore size of the TpPa-SO_3Na membrane is about 1.40 nm, which is close to their theoretical pore size of 1.41 nm (Fig. 3c).

The permanent porosity of TpPa-SO_3Na was assessed by nitrogen sorption isotherm at 77 K. The anionic COF membrane showed type I

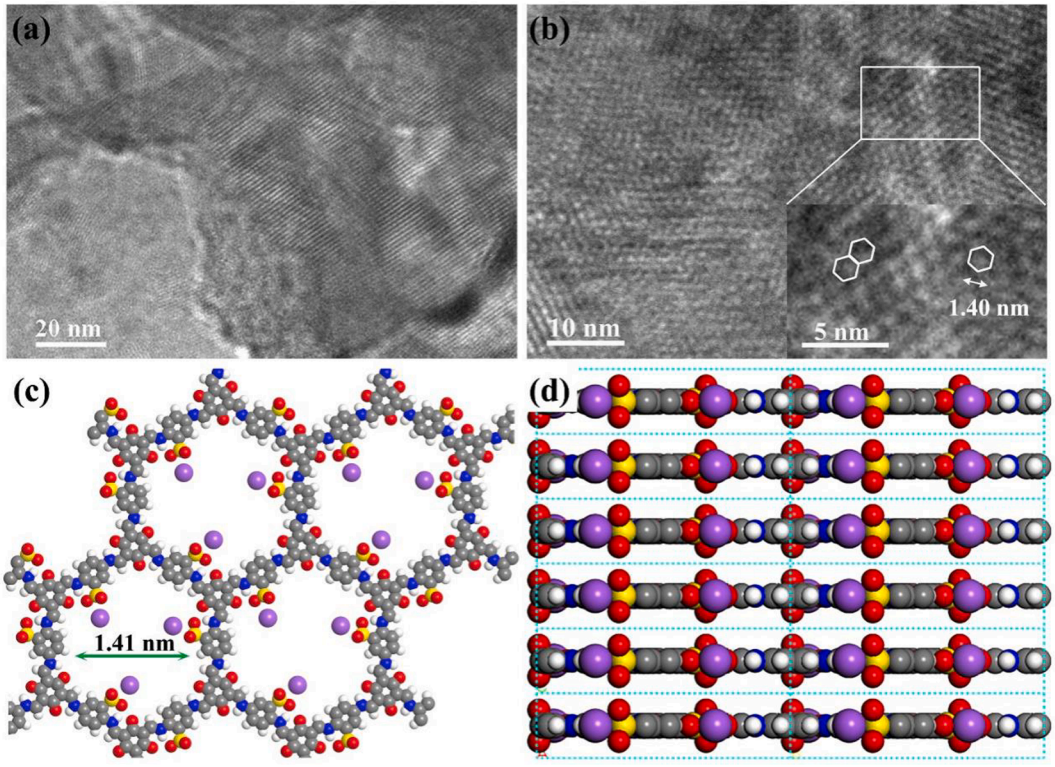

Fig. 3. (a) and (b) are TEM images of TpPa-SO_3Na membrane; (c) Crystal structure model of TpPa-SO_3Na membrane is shown for AA stacking mode; (d) Side view of the AA-stacking model structure of TpPa-SO_3Na membrane.

reversible N_2 adsorption–desorption (Fig. S5), which means the TpPa-SO_3Na COF is microporous framework (Fig. 3c and Fig. S6a). Moreover, the calculated Brunauer-Emmett-Teller (BET) surface area for TpPa-SO_3Na membrane is 212.3 $m^2 \cdot g^{-1}$. The lower surface area of TpPa-SO_3Na compared with TpPa-COF may be because the existence of -SO_3Na groups in the pore. Pore size distribution of TpPa-SO_3Na COF calculated by nonlocal density functional theory (NLDFT) reveals the COF have narrow pore size distribution located at 1.39 nm (Fig. S7). The PXRD was also performed to assess the crystallinity of TpPa-SO_3Na COF membrane. As shown in Fig. S8, TpPa-SO_3Na COF membrane exhibited an XRD peak at ~4.6°, corresponding to (100) reflection planes. Another broader peak also appeared at ~26.7°, which is attributed to π-π stacking resulting from the (001) planes (Fig. S8, blue curve) [41].

Contact angle experiments were performed to estimate the hydrophilicity of the membrane [43]. As displayed in Fig. 4a, b, the initial contact angles of water and acetonitrile on membrane surface are 40.5° and 32.8°, respectively. Obviously, the contact angles of both water and organic solvent on the membrane surface are much less than 90°, which indicates that the membrane has excellent amphiphilicity. The amphiphilicity of the membrane is very important for application in water and organic complex solvent filtration. Moreover, we also studied the surface charge characteristics of the membrane. As shown in Fig. 4c, the average Zeta potential on the surface of TpPa-SO_3Na membrane is −58.02 mV. The negative Zeta potential of membrane mainly arises from the electronegative -SO_3^- group.

3.2. Nanofiltration experiments

In view of above excellent properties of TpPa-SO_3Na membrane, we use the membrane for solvent filtration experiments. As shown in Fig. 5, TpPa-SO_3Na membrane shows remarkable permeability towards protic solvents, such as ethanol (223 L m^{-2} h^{-1} bar^{-1}), methanol (440 L m^{-2} h^{-1} bar^{-1}). As shown in Fig. 5a and Table S1, as the size of solvent molecules increases, their permeability was decreased. The exception of water permeability in protic solvents in COF membrane mainly caused by the difference in viscosity of these protic solvents. The viscosities of alcohols are related to molecule weight: methanol (0.5513 mPa·s), ethanol (0.7893 mPa·s), 1-propanol (1.943 mPa·s), 1-butanol (2.571 mPa·s), 1-pentanol (3.513 mPa·s) and 1-hexanol (4.590 mPa·s). But for water, the viscosity (η = 0.8937 mPa·s) is higher than methanol and ethanol, but lower than 1-propanol, 1-butanol, 1-pentanol, 1-hexanol due to their intermolecular hydrogen bonds. Moreover, the -SO_3Na group on the COF's pore surface is hydrophilic, which can also form hydrogen bonds with water. The hydrogen bond interactions between COF's pore surface and water may also lead to the decrease of water flux. We also studied the permeability of aprotic solvents in the membrane. The membrane displays higher permeability towards organic aprotic solvents than that of protic solvents (Fig. 5b and Table S2). For example, the permeability of the membrane to acetonitrile is 980 Lm^{-2} h^{-1} bar^{-1}. Moreover, the solvent permeabilities of TpPa-SO_3Na COF membrane are much higher than the existing nanofiltration membranes (Table S3 for details). The high solvent permeability and the differences between aprotic solvents and protic solvents can be attributed to: 1) The aprotic solvents have a lower viscosity than those protic solvents [28,44]; 2) Dipole interaction is weak between the aprotic solvents and the charged channels in TpPa-SO_3Na membrane; 3) TpPa-SO_3Na membrane has the high porosity and vertically aligned 1D channels in the direction of solvents migration which can reduce their diffusional resistance. We also assessed the effect of membrane thickness and pressure to the water permeance. Three membranes with different thickness (2.2, 2.8 and 3.5 μm) were used to water permeance. The water permeability decreases gradually as the increase of membrane thickness (Fig. 5c). Pressure-dependent water permeation result demonstrates that the water permeation is increased with pressure, as displayed in Fig. 5d.

Using porous membrane to recycle the valuable dyes is an economical but challenging approach as dyes usually have similar molecular sizes [45]. The high solvent permeability and electronegativity nature of TpPa-SO_3Na COF membrane motivated us to explore its potential applications in recycling valuable dyes. Several organic dyes with different charge including cationic dyes: Methylene blue (MB) and Ethidium bromide (EB); Neutral molecules: Nile red (NR) and p-Nitroaniline (NA); Anionic dyes: Methyl orange (MO) and Fluorescein Sodium salt (FSs) were employed for the separation study. The chemical structures, molecular sizes and charge properties of these dye molecules are displayed in Fig. S9 and Table S4, respectively.

The separation performance of TpPa-SO_3Na membrane towards pure dye solutions were evaluated firstly and the results were shown in Fig. 6. Consider the difference in solubility, negative and positive dyes can be completely dissolved in water, but neutral dyes can be completely dissolved in methanol instead of water.

As displayed in Fig. 6a, b, the characteristic absorption bands of two cationic dyes (MB, EB) dissolved in water are completely disappeared after filtration through the membrane, which indicates that the anionic TpPa-SO_3Na membrane can thoroughly intercept the cationic dye molecules. For anionic molecules water solution (MO, FSs), the absorption spectra intensity of two filtrates is significantly decreased compared to that of the feeding solutions, as shown in Fig. 6e, f. The absorption spectra intensity for two neutral molecules after filtering decreased slightly, which can be seen clearly in Fig. 6c, d. For more intuitively, the color change of dye solutions before and after filtration (under visible light) was shown in Fig. 6 inset, respectively. Visibly, for cationic dyes, two filtrates are completely colorless (Fig. 6a, b inset). However, the filtrates obtained from anionic dyes (MO, FSs) (Fig. 6e, f inset) still retain some of their colors. This suggests that a portion of dye molecules have penetrated through the membrane. By comparison, neutral dyes methanol solution (NR, NA) (Fig. 6c, d inset) still retain deep color,

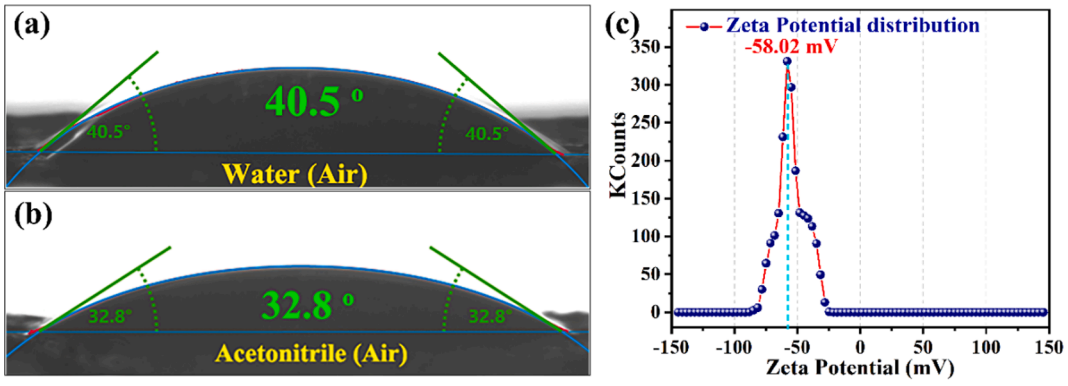

Fig. 4. (a) and (b) are the contact angles of TpPa-SO_3Na COF membrane to water and acetonitrile, respectively; (c) The average Zeta potential of TpPa-SO_3Na membrane.

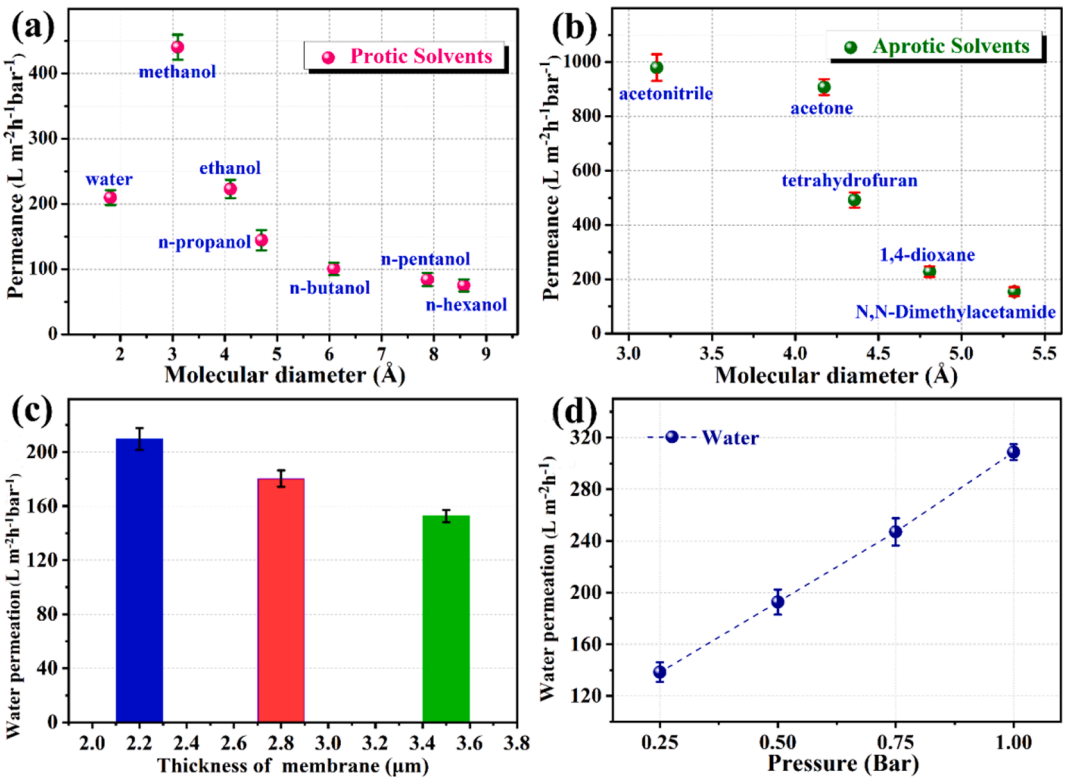

Fig. 5. Pure solvent permeance versus molecular diameter of different protic solvents (a) and aprotic solvents (b); (c) Comparison of the water permeation of TpPa-SO_3Na membrane with different thickness; (d) Pressure-dependent water permeation study of TpPa-SO_3Na membrane.

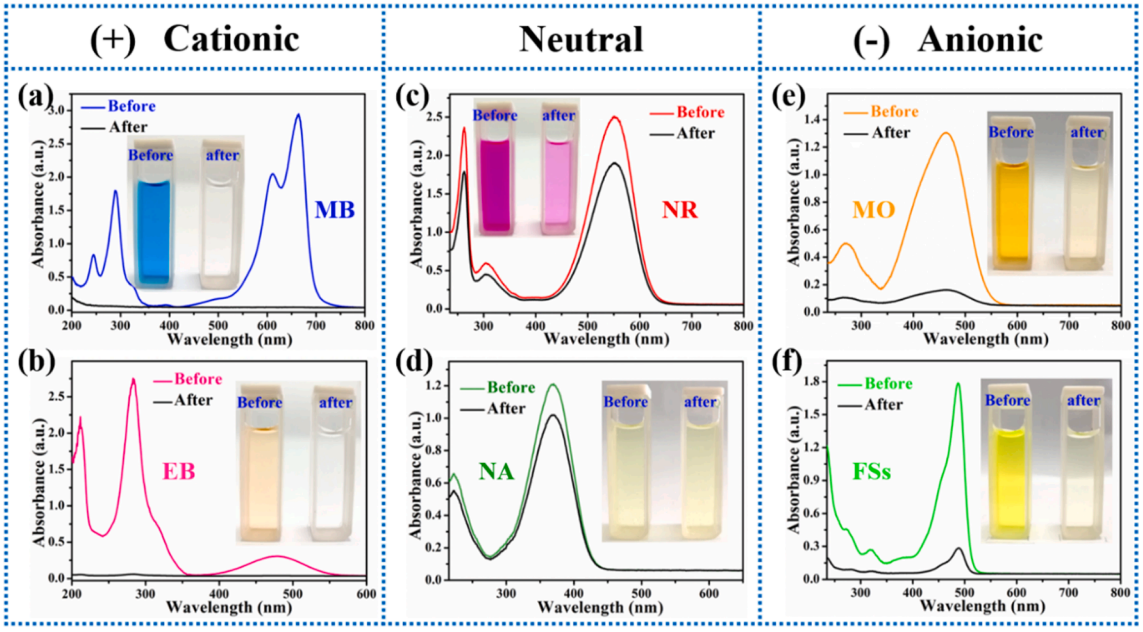

Fig. 6. Charge- and size-selective separation experiments. (a-f) UV–vis absorption spectra and the corresponding photographs of different dyes solutions before and after filtration through TpPa-SO_3Na membrane: (a) Methylene blue (MB) with a size of 5.63 × 14.21 Å, Solvent: Water; (b) Ethidium bromide (EB) with a size of 9.15 × 11.04 Å, Solvent: Water; (c) Nile red (NR) with a size of 6.51 × 14.12 Å, Solvent: Methanol; (d) p-Nitroaniline (NA) with a size of 4.32 × 6.89 Å, Solvent: Methanol; (e) Methyl orange (MO) with a size of 5.19 × 14.62 Å, Solvent: Water; (f) Fluorescein Sodium salt (FSs) with a size of 9.64 × 10.34 Å, Solvent: Water; respectively.

which implies that the membrane has a poor rejection performance against the neutral dyes molecule.

Further, the rejection values of TpPa-SO_3Na membrane towards different dyes were quantitatively calculated according to the Beer-Lambert law. As shown in Fig. 7a, the anionic TpPa-SO_3Na membrane can reject 99.8% and 99.5% cationic MB and EB respectively. Whereas the interception efficiency for anionic MO and FSs is 87.6% and 84.1%, respectively. By contrast, the membrane exhibits very low rejection performance for neutral dyes: the rejection values of the membrane for NR and NA are only 24.4% and 16.7%, respectively. A systematic

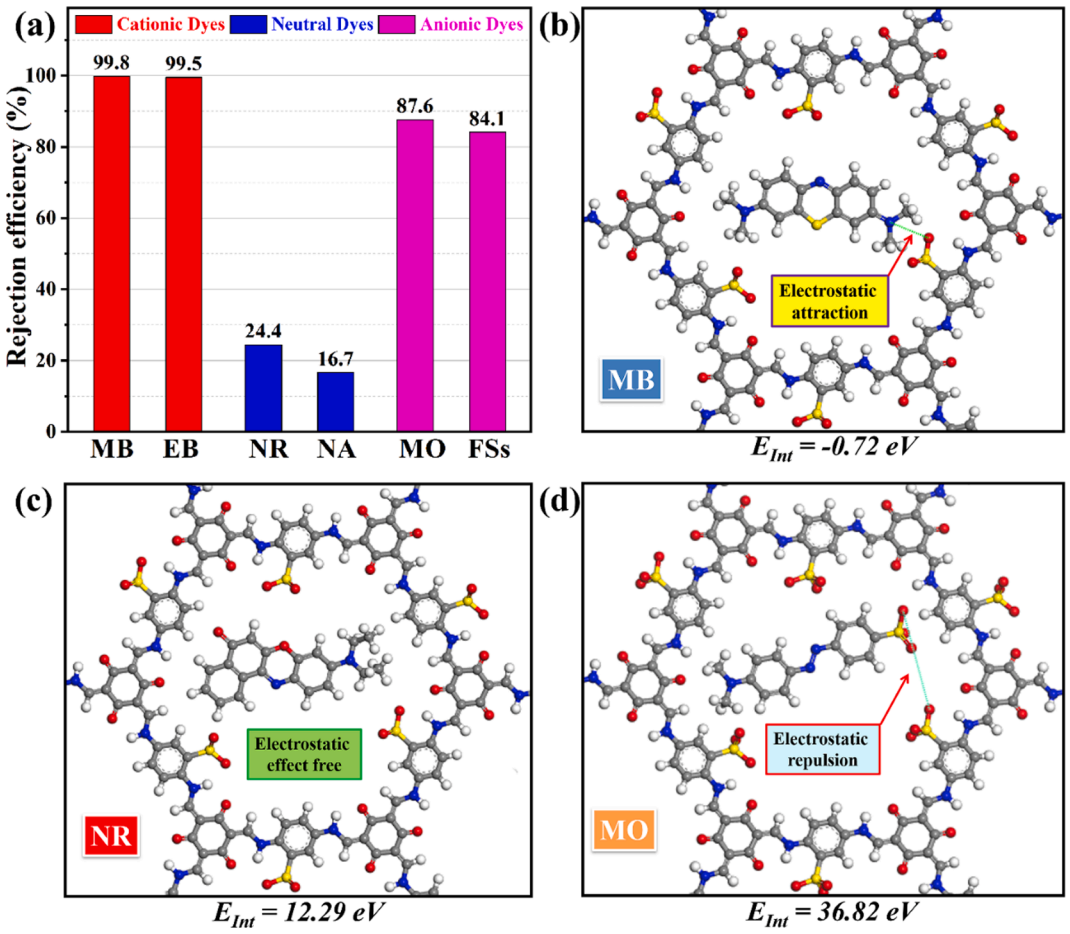

Fig. 7. (a) The rejection efficiency of TpPa-SO_3Na membrane towards different dyes. Simulated model and interaction energy (E_{Int}) of composite consisting of TpPa-SO_3Na membrane and dye molecules: (b) Membrane and MB (cationic) composite; (c) Membrane and NR (neutral) composite; (d) Membrane and MO (anionic) composite.

comparison of the sieving performance of TpPa-SO_3Na membrane with other membrane materials toward cationic dyes was performed, as displayed in Table S5.

The above experimental results demonstrate that the TpPa-SO_3Na membrane has discrepant molecular interception ability for the dyes with different charge. The anionic sites in the membrane may play a critical role in the dyes separation process [38,46]. In order to further understand the selective separation behaviors of TpPa-SO_3Na membrane towards different charged molecules, we performed the theoretical calculation to verify the difference in interaction forces between membrane and different charged molecules. The DFT (Density functional theory) calculations basing on linear combination of atomic orbital (LCAO) were conducted using $DMol^3$ package of Material Studio [47,48]. The interaction energy (E_{Int}) (or called binding energy) between membrane and molecules is expressed by follow equation:

$$Me(Membrane) + Mo(Molecule) \Longleftrightarrow Me@Mo\ complex \quad (2)$$

The interaction energy E_{Int} was calculated by DFT calculation results using the follow equation:

$$E_{Int} = E_{Me@Mo\ complex} - E_{Me} - E_{Mo} - BSSE \quad (3)$$

In Eq. (3), the four terms on the right are respectively the total energy of the *Me@Mo* complex, the isolated membrane and molecule, and basis set superposition error (*BSSE*).

As shown in Fig. 7b, c, d, the E_{Int} values of cationic molecule (MB), neutral molecule (NR) and anionic molecule (MO) are −0.72 eV, 12.29 eV and 36.82 eV, respectively. Obviously, the value of E_{Int} between membrane and cationic MB is the lowest, indicating that there is the electrostatic attraction between membrane and cationic molecule. Thus the total energy of the complex is reduced. Moreover, the negative binding energy means membrane-cationic molecule combination is thermodynamically stable. By contrast, the E_{Int} between membrane and anionic MO is positive and the absolute value is much higher than that of other two combinations, which suggests that there is maybe electrostatic repulsion interaction between negatively charged membrane and anionic molecule. Therefore, the total energy of the composite is increased. For neutral molecule NR, the E_{Int} value lies between MB and MO, which is due to lack of electrostatic interaction between neutral molecule and membrane. The above theoretical calculation results accord with the coulomb interaction principle between charged matter [49,50]. Hence, integrating the ionic modules into the skeleton of COF membrane would clearly endue it the ability of identifying different charged molecules.

The dyes recycle experiment was also conducted to evaluate the selective molecular separation in TpPa-SO_3Na membrane. A mixed dye solutions consisting of MB (Methylene blue) and NA (p-Nitroaniline) was used to filter through the membrane. As shown in Fig. 8b, the turquoise feed solution (derived from MB and NA) changed in to light-green filtrate after the TpPa-SO_3Na membrane filteration. In addition, the Ultraviolet–visible spectra before and after the membrane treatment suggest that MB can be completely intercepted via the membrane, while NA concentration does not show any change (Fig. 8c). After we rinsing the MB-contained membrane with NaCl aqueous solution, we can recycle MB dye. This result confirmed that the anionic membrane can recycle cationic dyes molecule from a mixture effectively. In order to confirm the membrane separation ability, a more complex mixing

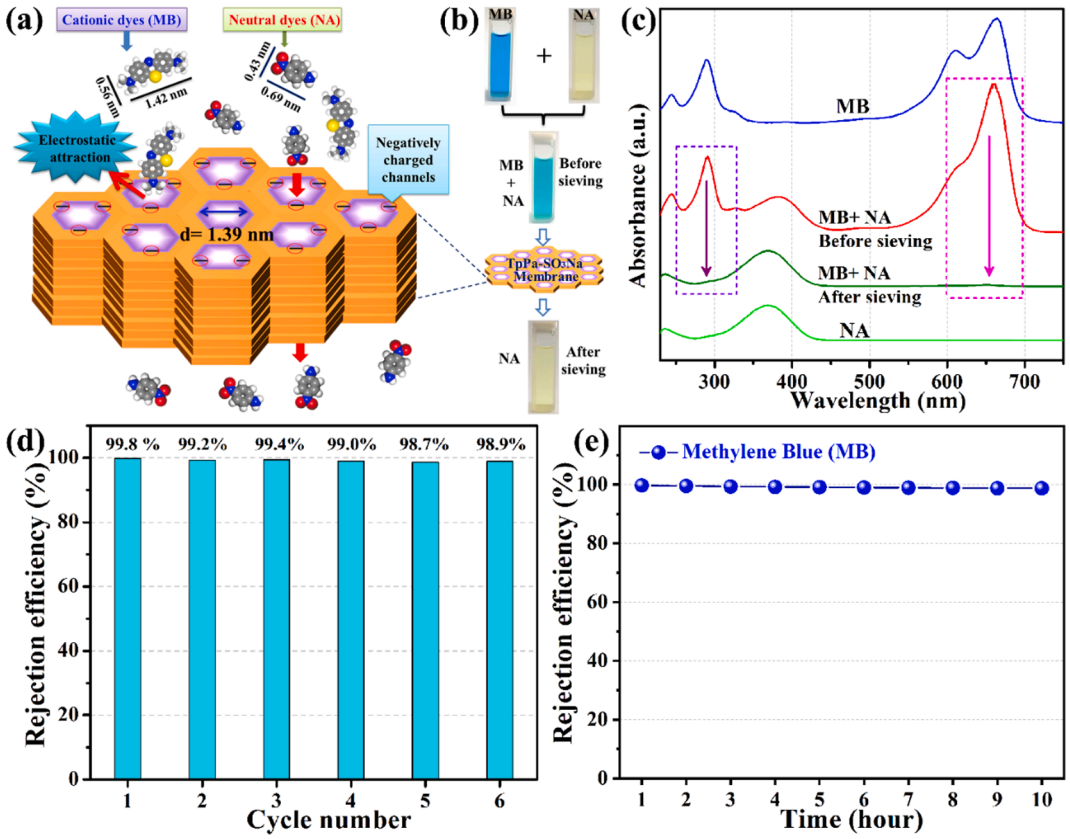

Fig. 8. (a) Schematic for molecular sieving mechanism through ordered-vertical arrayed 1D nanochannels with negative charge of TpPa-SO_3Na membrane; (b) Photo images show the selective sieving of methylene blue (MB) from a mixture of MB and NA; (c) The correspond Ultraviolet–visible spectra of the selective separation; (d) Cycle study of MB rejection through TpPa-SO_3Na membrane; (e) The time course of rejection efficiency of TpPa-SO_3Na membrane for MB aqueous solution.

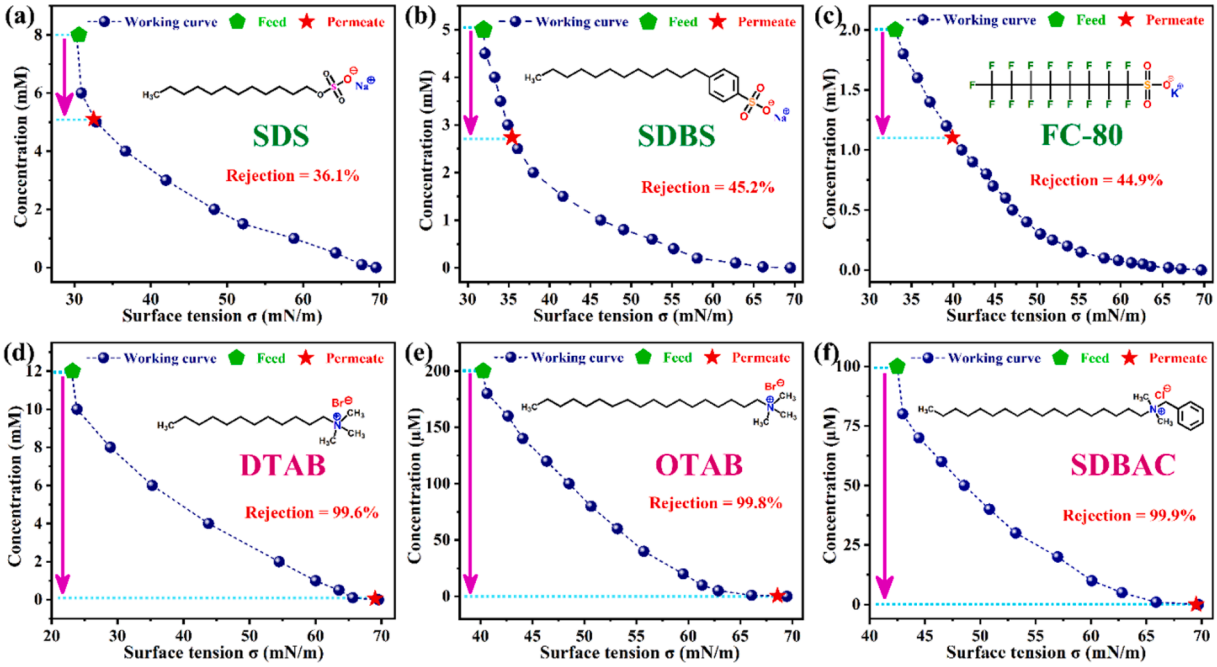

Fig. 9. The rejection efficiency of TpPa-SO_3Na membrane towards surfactants with different charges. **Anionic surfactants:** (a) Sodium dodecyl sulfate (SDS); (b) Sodium dodecyl benzene sulfonate (SDBS); (c) Perfluorooctanesulfonic acid potassium salt (FC-80). **Cationic surfactants:** (d) Dodecyl trimethyl ammonium bromide (DTAB); (e) Octadecyltrimethylammonium bromide (OTAB); (f) Stearyldimethylbenzylammonium chloride (SDBAC).

solution, consisting of three dyes with different charge properties, was also conducted. As shown in Fig. S10, the mixing dye solution [MB (cationic), NA (neutral) and FSs (anionic)] was filtered through TpPa-SO_3Na membrane. The color of the mixing solution changes from dark green to pistac (Fig. S10a). Correspondingly, the absorption spectra of solution before and after filtration also verified the cationic dye separation performance of the membrane (Fig. S10b).

The recyclability and durability of the membrane are very important in the practical application. Therefore, a cycle rejection study of TpPa-SO_3Na COF membrane for MB was executed. As displayed in Fig. 8d and Fig. S11, the rejection value of the recycled TpPa-SO_3Na membrane for MB retains 98.9% of the original capacity even after six cycles. Subsequently, the durability of the TpPa-SO_3Na membrane was also investigated by recording the time course of rejection efficiency of TpPa-SO_3Na membrane for cationic dye (MB). As we can see in Fig. 8e, the membrane can still retain the rejection efficiency for MB above 98.8% after 10 h operation.

Based on the above performance of TpPa-SO_3Na COF membrane, we employed it to dispose another kind of intractable organic pollutant–surfactants. Surfactants are widely used in industrial processes such as corrosion inhibition, dispersion stabilization, detergency, crude oil refining and lubrication [51–54]. A large amount of surfactant-containing wastewater will inevitably be produced, and the disorderly discharge of these wastewater will cause great harm to the ecological environment and human health [55–57]. The amphiphilicity and micelle forming nature in water of surfactants lead to traditional nanofiltration membranes are ineffective to separate them. The charged TpPa-SO_3Na membrane may provide an effective way to demulsify and remove surfactants from water. Herein, several common surfactants are selected to test the removal performance of the TpPa-SO_3Na membrane. As displayed in Fig. 9, the rejection efficiency of the membrane towards surfactants with different charged is significantly different. For anionic-surfactants, the membrane can only intercept 36.1% SDS, 45.2% SDBS and 44.9% FC-80, respectively (Fig. 9a, b, c). By comparison, the membrane exhibits very excellent rejection performance for cationic-surfactants, the rejection values of DTAB, OTAB and SDBAC are up to 99.6%, 99.8% and 99.9%, respectively (Fig. 9d, e, f). The results clearly show that TpPa-SO_3Na membrane can selectively remove cationic surfactants efficiently.

4. Conclusions

In conclusion, we have successfully prepared a sulfonate (-SO_3Na) functionalized 2D anionic COF membrane by interfacial crystallization approach. Integrating ionic module in nanopore renders TpPa-SO_3Na COF membrane with specific electronegativity compared with previous neutral COF membranes. The synergy between electrostatic interaction and molecular size sieving effect in TpPa-SO_3Na membrane endows the membrane excellent separation ability towards organic pollutant molecules with different charges. Excitingly, the TpPa-SO_3Na membrane can effectively recycle $>$ 99% of cationic molecules, while maintaining excellent solvent permeability. These results demonstrated that anionic COF membrane can provide a new efficient charge-driven separation method for organic pollutants removal, which may guide membrane materials design for precise charge-dependent molecular sieving in mixture separation in future.

CRediT authorship contribution statement

Tongfan Chen: Investigation, Data curation, Writing - original draft, Writing - review & editing. **Bin Li:** Conceptualization, Methodology. **Wenbo Huang:** Visualization. **Chunhui Lin:** Visualization. **Guangshe Li:** Methodology, Validation. **Hao Ren:** Methodology, Validation. **Yue Wu:** Software, Formal analysis. **Shuhui Chen:** Software, Formal analysis. **Wenxiang Zhang:** Investigation, Data curation, Writing - original draft, Writing - review & editing. **Heping Ma:** Supervision.

Declaration of Competing Interest

The authors declare that they have no known competing financial interests or personal relationships that could have appeared to influence the work reported in this paper.

Acknowledgements

This work was supported by National Natural Science Foundation of China (Grant No. 21773223, 21673218, 51872281) and the Science and Technology Developing Project of Jilin Province (Grant No. 20180101177JC, 20180101176JC). This work was also supported by the Natural Science Basic Research Plan in Shaanxi Province of China (No. 2020JM-005 and 2020JQ-017). The authors also thank the Open Funds of State Key Laboratory of Inorganic Synthesis and Preparative Chemistry, Jilin University. Prof. H. Ma thanks the Fundamental Research Funds for "Young Talent Support Plan" of Xi'an Jiaotong University (HG6J001), the Fundamental Research Funds for the Central Universities (xzy012019027) and "1000-Plan program" of Shaanxi province. The authors also gratefully acknowledge Prof. Huanyu Zhao at Jilin University for help in getting access to the software of Materials Studio.

Appendix A. Supplementary data

Supplementary data to this article can be found online at https://doi.org/10.1016/j.seppur.2020.117787.

References

[1] A. Alsbaiee, B.J. Smith, L. Xiao, Y. Ling, D.E. Helbling, W.R. Dichtel, Rapid removal of organic micropollutants from water by a porous β-cyclodextrin polymer, Nature 529 (7585) (2016) 190–194.
[2] R.P. Schwarzenbach, B.I. Escher, K. Fenner, T.B. Hofstetter, C.A. Johnson, U. Von Gunten, B. Wehrli, The challenge of micropollutants in aquatic systems, Science 313 (2006) 1072–1077.
[3] C. Grandclément, I. Seyssiecq, A. Piram, P. Wong-Wah-Chung, G. Vanot, N. Tiliacos, N. Roche, P. Doumenq, From the conventional biological wastewater treatment to hybrid processes, the evaluation of organic micropollutant removal: a review, Water Res. 111 (2017) 297–317.
[4] T. Shen, M. Gao, Gemini surfactant modified organo-clays for removal of organic pollutants from water: a review, Chem. Eng. J. 375 (2019) 121910, https://doi.org/10.1016/j.cej.2019.121910.
[5] S. Xie, S. Wu, S. Bao, Y. Wang, Y. Zheng, D. Deng, L. Huang, L. Zhang, M. Lee, Z. Huang, Intelligent mesoporous materials for selective adsorption and mechanical release of organic pollutants from water, Adv. Mater. 30 (2018) 1800683.
[6] X. Duan, C. Zhang, S. Wang, N. Ren, S.-H. Ho, Graphitic biochar catalysts from anaerobic digestion sludge for nonradical degradation of micropollutants and disinfection, Chem. Eng. J. 384 (2020) 123244.
[7] M.M. Pendergast, E.M.V. Hoek, A review of water treatment membrane nanotechnologies, Energy Environ. Sci. 4 (6) (2011) 1946, https://doi.org/10.1039/c0ee00541j.
[8] A.W. Mohammad, Y.H. Teow, W.L. Ang, Y.T. Chung, D.L. Oatley-Radcliffe, N. Hilal, Nanofiltration membranes review: recent advances and future prospects, Desalination 356 (2015) 226–254.
[9] C. Castel, E. Favre, Membrane separations and energy efficiency, J. Membr. Sci. 548 (2018) 345–357.
[10] J.R. Werber, C.O. Osuji, M. Elimelech, Materials for next-generation desalination and water purification membranes, Nat Rev Mater 1 (5) (2016), https://doi.org/10.1038/natrevmats.2016.18.
[11] A. Lee, J.W. Elam, S.B. Darling, Membrane materials for water purification: design, development, and application, Environ. Sci. Water Res. Technol. 2 (2016) 17–42.
[12] M. Paul, S.D. Jons, Chemistry and fabrication of polymeric nanofiltration membranes: a review, Polymer 103 (2016) 417–456.
[13] J. Yin, B. Deng, Polymer-matrix nanocomposite membranes for water treatment, J. Membr. Sci. 479 (2015) 256–275.
[14] P. Marchetti, M.F. Jimenez Solomon, G. Szekely, A.G. Livingston, Molecular separation with organic solvent nanofiltration: a critical review, Chem. Rev. 114 (21) (2014) 10735–10806.
[15] J. Wu, F. Xu, S. Li, P. Ma, X. Zhang, Q. Liu, R. Fu, D. Wu, Porous polymers as multifunctional material platforms toward task-specific applications, Adv. Mater. 31 (2019) 1802922.
[16] N. Prasetya, N.F. Himma, P.D. Sutrisna, I.G. Wenten, B.P. Ladewig, A review on emerging organic-containing microporous material membranes for carbon capture and separation, Chem. Eng. J. 391 (2020) 123575, https://doi.org/10.1016/j.cej.2019.123575.

[17] J. Wang, J. Zhu, Y. Zhang, J. Liu, B. Van der Bruggen, Nanoscale tailor-made membranes for precise and rapid molecular sieve separation, Nanoscale 9 (9) (2017) 2942–2957.
[18] J. Liu, D. Hua, Y. Zhang, S. Japip, T. Chung, Precise molecular sieving architectures with janus pathways for both polar and nonpolar molecules, Adv. Mater. 30 (2018) 1705933.
[19] S. Kim, K.H. Chu, Y.A.J. Al-Hamadani, C.M. Park, M. Jang, D.-H. Kim, M. Yu, J. Heo, Y. Yoon, Removal of contaminants of emerging concern by membranes in water and wastewater: a review, Chem. Eng. J. 335 (2018) 896–914.
[20] S. Kandambeth, K. Dey, R. Banerjee, Covalent organic frameworks: chemistry beyond the structure, J. Am. Chem. Soc. 141 (5) (2019) 1807–1822.
[21] J.L. Segura, M.J. Mancheño, F. Zamora, Covalent organic frameworks based on Schiff-base chemistry: synthesis, properties and potential applications, Chem. Soc. Rev. 45 (2016) 5635–5671.
[22] S. Cao, B. Li, R. Zhu, H. Pang, Design and synthesis of covalent organic frameworks towards energy and environment fields, Chem. Eng. J. 355 (2019) 602–623.
[23] N. Huang, P. Wang, D. Jiang, Covalent organic frameworks: a materials platform for structural and functional designs, Nat. Rev. Mater. 1 (2016) 1–19.
[24] R.P. Bisbey, W.R. Dichtel, Covalent organic frameworks as a platform for multidimensional polymerization, ACS Cent. Sci. 3 (6) (2017) 533–543.
[25] U. Díaz, A. Corma, Ordered covalent organic frameworks, COFs and PAFs. From preparation to application, Coord. Chem. Rev. 311 (2016) 85–124.
[26] S. Yuan, X. Li, J. Zhu, G. Zhang, P. Van Puyvelde, B. Van der Bruggen, Covalent organic frameworks for membrane separation, Chem. Soc. Rev. 48 (10) (2019) 2665–2681.
[27] M. Matsumoto, L. Valentino, G.M. Stiehl, H.B. Balch, A.R. Corcos, F. Wang, D. C. Ralph, B.J. Mariñas, W.R. Dichtel, Lewis-acid-catalyzed interfacial polymerization of covalent organic framework films, Chem 4 (2) (2018) 308–317.
[28] S. Kandambeth, B.P. Biswal, H.D. Chaudhari, K.C. Rout, S. Kunjattu H, S. Mitra, S. Karak, A. Das, R. Mukherjee, U.K. Kharul, Selective molecular sieving in self-standing porous covalent-organic-framework membranes, Adv. Mater. 29 (2017) 1603945.
[29] T. Wang, H. Wu, S. Zhao, W. Zhang, M. Tahir, Z. Wang, J. Wang, Interfacial polymerized and pore-variable covalent organic framework composite membrane for dye separation, Chem. Eng. J. 384 (2020) 123347.
[30] D. Xu, J. Guo, F. Yan, Porous ionic polymers: Design, synthesis, and applications, Prog. Polym. Sci. 79 (2018) 121–143.
[31] Tao Luo, Said Abdu, Matthias Wessling, Selectivity of ion exchange membranes: a review, J. Membr. Sci. 555 (2018) 429–454.
[32] A.R. Koltonow, J. Huang, Two-dimensional nanofluidics, Science 351 (6280) (2016) 1395–1396.
[33] Jeehye Byun, Hasmukh A. Patel, Damien Thirion, Cafer T. Yavuz, Charge-specific size-dependent separation of water-soluble organic molecules by fluorinated nanoporous networks, Nat. Commun. 7 (1) (2016), https://doi.org/10.1038/ncomms13377.
[34] Xingyu Lin, Qian Yang, Longhua Ding, Bin Su, Ultrathin silica membranes with highly ordered and perpendicular nanochannels for precise and fast molecular separation, ACS Nano 9 (11) (2015) 11266–11277.
[35] Qi Wen, Dongxiao Yan, Feng Liu, Mao Wang, Yun Ling, Pengfei Wang, Patrick Kluth, Daniel Schauries, Christina Trautmann, Pavel Apel, Wei Guo, Guoqing Xiao, Jie Liu, Jianming Xue, Yugang Wang, Highly selective ionic transport through subnanometer pores in polymer films, Adv. Funct. Mater. 26 (32) (2016) 5796–5803.
[36] Hongwei Fan, Jiahui Gu, Hong Meng, Alexander Knebel, Jürgen Caro, High-flux membranes based on the covalent organic framework COF-LZU1 for selective dye separation by nanofiltration, Angew. Chem. Int. Ed. 57 (15) (2018) 4083–4087.
[37] S. Karak, K. Dey, A. Torris, A. Halder, S. Bera, F. Kanheerampockil, R. Banerjee, Inducing disorder in order: hierarchically porous covalent organic framework nanostructures for rapid removal of persistent organic pollutants, J. Am. Chem. Soc. 141 (2019) 7572–7581.
[38] N. Huang, P. Wang, M.A. Addicoat, T. Heine, D. Jiang, Ionic covalent organic frameworks: design of a charged interface aligned on 1D channel walls and its unusual electrostatic functions, Angew. Chemie Int. Ed. 56 (2017) 4982–4986.
[39] Qing Chen, Pingping Yu, Wenqiang Huang, Sanchuan Yu, Meihong Liu, Congjie Gao, High-flux composite hollow fiber nanofiltration membranes fabricated through layer-by-layer deposition of oppositely charged crosslinked polyelectrolytes for dye removal, J. Membr. Sci. 492 (2015) 312–321.
[40] Kaushik Dey, Manas Pal, Kanhu Charan Rout, Shebeeb Kunjattu H, Anuja Das, Rabibrata Mukherjee, Ulhas K. Kharul, Rahul Banerjee, Selective molecular separation by interfacially crystallized covalent organic framework thin films, J. Am. Chem. Soc. 139 (37) (2017) 13083–13091.
[41] Suman Chandra, Tanay Kundu, Kaushik Dey, Matthew Addicoat, Thomas Heine, Rahul Banerjee, Interplaying intrinsic and extrinsic proton conductivities in covalent organic frameworks, Chem. Mater. 28 (5) (2016) 1489–1494.
[42] Yongwu Peng, Guodong Xu, Zhigang Hu, Youdong Cheng, Chenglong Chi, Daqiang Yuan, Hansong Cheng, Dan Zhao, Mechanoassisted synthesis of sulfonated covalent organic frameworks with high intrinsic proton conductivity, ACS Appl. Mater. Interfaces 8 (28) (2016) 18505–18512.
[43] Guo-dong Kang, Yi-ming Cao, Application and modification of poly(vinylidene fluoride) (PVDF) membranes – a review, J. Membr. Sci. 463 (2014) 145–165.
[44] I. Avramov, Relationship between diffusion, self-diffusion and viscosity, J. Non-Cryst. Solids 355 (10-12) (2009) 745–747.
[45] Zhigao Zhu, Ping Wu, Guojuan Liu, Xiaofan He, Benyu Qi, Gaofeng Zeng, Wei Wang, Yuhan Sun, Fuyi Cui, Ultrahigh adsorption capacity of anionic dyes with sharp selectivity through the cationic charged hybrid nanofibrous membranes, Chem. Eng. J. 313 (2017) 957–966.
[46] H. Ma, B. Liu, B. Li, L. Zhang, Y.-G. Li, H.-Q. Tan, H.-Y. Zang, G. Zhu, Cationic covalent organic frameworks: a simple platform of anionic exchange for porosity tuning and proton conduction, J. Am. Chem. Soc. 138 (2016) 5897–5903.
[47] Peng Zhang, Qichen Zhao, Jingjun Liu, Bolun Yang, Research on inhibitors and hindered groups in ultra-deep hydrodesulfurization based on density functional theory, Catal. Today 314 (2018) 170–178.
[48] Ce Zhang, Lei Wang, Guillaume Maurin, Qingyuan Yang, In Silico Screening of MOFs with open copper sites for C 2 H 2 /CO 2 separation, AIChE J 64 (11) (2018) 4089–4096.
[49] Mehrdad Taheran, Satinder K. Brar, M. Verma, R.Y. Surampalli, T.C. Zhang, J. R. Valero, Membrane processes for removal of pharmaceutically active compounds (PhACs) from water and wastewaters, Sci. Total Environ. 547 (2016) 60–77.
[50] Y. Li, Z. Yang, Y. Wang, Z. Bai, T. Zheng, X. Dai, S. Liu, D. Gui, W. Liu, M. Chen, A mesoporous cationic thorium-organic framework that rapidly traps anionic persistent organic pollutants, Nat. Commun. 8 (2017) 1–11.
[51] Trygve Dagsloth Jakobsen, Sébastien Simon, Ellinor Bævre Heggset, Kristin Syverud, Kristofer Paso, Interactions between surfactants and cellulose nanofibrils for enhanced oil recovery, Ind. Eng. Chem. Res. 57 (46) (2018) 15749–15758.
[52] Asamanjoy Bhunia, Subarna Dey, Maria Bous, Chenyang Zhang, Wolfgang von Rybinski, Christoph Janiak, High adsorptive properties of covalent triazine-based frameworks (CTFs) for surfactants from aqueous solution, Chem. Commun. 51 (3) (2015) 484–486.
[53] Max J. Klemes, Yuhan Ling, Casey Ching, Congyue Wu, Leilei Xiao, Damian E. Helbling, William R. Dichtel, Reduction of a tetrafluoroterephthalonitrile-β-cyclodextrin polymer to remove anionic micropollutants and perfluorinated alkyl substances from water, Angew. Chem. 131 (35) (2019) 12177–12181.
[54] Stefanía Betancur, Francisco Carrasco-Marín, Camilo A. Franco, Farid B. Cortés, Development of composite materials based on the interaction between nanoparticles and surfactants for application in chemical enhanced oil recovery, Ind. Eng. Chem. Res. 57 (37) (2018) 12367–12377.
[55] James K. Johnson, Christopher M. Hoffman Jr., Douglas A. Smith, Zhiyong Xia, Advanced filtration membranes for the removal of perfluoroalkyl species from water, ACS Omega 4 (5) (2019) 8001–8006.
[56] D.Q. Zhang, W.L. Zhang, Y.N. Liang, Adsorption of perfluoroalkyl and polyfluoroalkyl substances (PFASs) from aqueous solution-A review, Sci. Total Environ. 694 (2019) 133606.
[57] Woojung Ji, Leilei Xiao, Yuhan Ling, Casey Ching, Michio Matsumoto, Ryan P. Bisbey, Damian E. Helbling, William R. Dichtel, Removal of GenX and perfluorinated alkyl substances from water by amine-functionalized covalent organic frameworks, J. Am. Chem. Soc. 140 (40) (2018) 12677–12681.